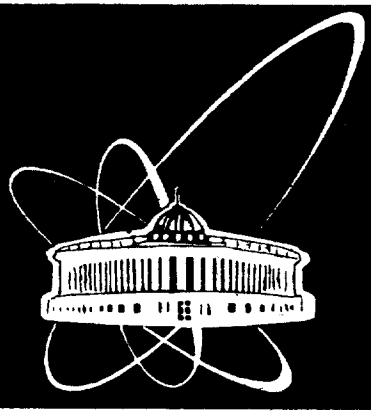

ОБЪЕДИНЕННЫЙ
ИНСТИТУТ
ЯДЕРНЫХ
ИССЛЕДОВАНИЙ

Дубна

BB

E15-96-365

Yu.V.Pyatkov[1], V.V.Pashkevich, Yu.E.Penionzhkevich,
V.G.Tishchenko, A.V.Unzhakova, H.-G.Ortlepp[2],
P.Gippner[2], C.-M.Herbach[2], W.Wagner[2]

MANIFESTATION OF CLUSTERING IN THE $^{252}Cf\,(sf)$ AND $^{249}Cf\,(n_{th},f)$ REACTIONS

Submitted to «Nuclear Physics A»

SW9712

[1]Moscow Engineering Physics Institute, 115409 Moscow, Russia
[2]Forschungszentrum Rossendorf e.V., D-01314 Dresden, Germany

1996

1 Introduction

Some recent investigations of the spontaneously fissioning nucleus of ^{252}Cf provide new, non-trivial results concerning the two extreme situations in nuclear fission, namely, on the true cold fission [1] and fission from the hyperdeformed states of the fissioning system [2]. The role of these phenomena in understanding the full picture of the process should be a subject of through attention. In the present-day models of fission at low excitation energies the cold fission events or cold fragmentation (CF) are treated as extreme events, taking place at the phase-space boundaries of the fissioning system [3]. In the popular model proposed by Brosa et al. [4] such events are considered to be the tails of the conventional kinetic energy distributions of fission fragments (FF). The models giving qualitative [5] and quantitative description of the CF [6] do not associate cold fission with a general evolution of the nuclear shape in the fission process either. At the same time as it follows from [7] the CF can play the role of a specific spectator of this evolution at the initial or final (for deformed CF) stage of the process. Therefor the mass-energy distributions of the CF products should contain information concerning the shape of the fissioning nucleus for different fission modes at the initial and final stages of the descent from the fission barrier.

The present paper aims at extracting such information from the mass-energy distributions measured experimentally and at making its analysis using potential energy surface (PES) calculations for the two isotopes ^{252}Cf and ^{250}Cf.

The comparison of experimental findings and theoretical predictions in two opposite limits of the descent path proves to be a rigorous test for the valleys structure obtained in the PES calculations.

2 Experiment

The success of investigations mentioned in [1, 2] was conditioned by the use of high efficiency experimental set-ups. The 4π-spectrometer of charged fragments, FOBOS, mounted in FLNR JINR [8] is an example of such a device. In this facility the informative but low-efficiency method of measuring primary fragment masses according to two velocities (the $2V$-method) is performed as a mosaic detector consisting of thirty

modules that cover an angle close to 4π.

The present experiment has been performed using two modules of the FOBOS array [8], each consisting of a position-sensitive double-grid avalanche counter (DGAC) and a Bragg ionization chamber (BIC). The velocity of a fission fragment (FF) has been determined by a microchannel-plate start detector [9] and DGAC stop signals (time-of-flight (TOF) paths of about 50 cm). The FF energies were measured in the BIC's. For each pair of fragments, the mass and momentum values have been obtained from the velocity and energy measurements, event-wise within a given interval, determined by the resolution and the neutron emission. Events not satisfying the selection rule were rejected. Thus, the peak-to-valley ratio in the mass distributions was increased from 34 to 52. As a result, the combined TOF-TOF and TOF-E analysis yields this ratio a factor of 2 better than the twin-ionization chamber method does [1]. A total number of 1.5×10^7 FF pairs satisfied the selection rule.

The improved spectrum obtained after rejecting of scattered events is shown in Fig. 1. Figs. 1a and 1b demonstrate the total kinetic energy-mass (TKE-M) distributions without and with rejection of false events, respectively. Fig. 2 shows FF mass spectra obtained in [10] and in this work for CF region. Such data are very sensitive to a mass-energy resolution and quality of calibration. The spectra depicted in Fig. 2 agree with each other.

The ^{249}Cf(n_{th},f) reaction was studied [11] using the time-of-flight spectrometer of unslowed fission products [12] at the MEPhI research reactor. The energy measurement was carried out with a gas-ionization chamber [13]. The energy calibration procedure was described in [14]. It is based on the well-known Schmitt parameterization for energy-amplitude-mass dependence. Coefficients for this formula were obtained as a result of the fitting the experimental FF mass distribution of the ^{235}U(n_{th},f) reaction to the tabulated one. The Californium target, about $20\,\mu g/cm^2$ thick, was produced by electrodepositing ^{249}Cf onto a stainless steel backing. The overall statistics collected in the experiment is 6×10^6 events. The integral mass yield distribution of fission fragments as well as the mass distributions of FF with fixed kinetic energies are in a good agreement with the previous results [15].

3 Experimental results

A comparative analysis of the results on ^{252}Cf as well as ^{250}Cf* fission presented in the same coordinates is given below. Fig. 3 displays the contour maps of TKE-M distributions of FF for ^{252}Cf and ^{250}Cf*. Equiprobability lines are drawn with a 4% step from the FF maximal yield of the light group. A qualitative difference between the distributions at high TKE values lies in the presence of a two-dimensional "bump" for ^{250}Cf* FF in the vicinity of the mass split with the heavy fragment mass $M_H \approx 132\,amu$.

A more detailed information concerning the nature of the difference can be extracted from FF yields spectra for fixed values of excitation energy, $E^* = Q - TKE$, where Q is the energy released in the reaction for a given mass split (Fig. 4). One can see that there is a shift of the ^{252}Cf FF spectra to the lighter masses. The most significant difference in the yields is observed for $A_H \approx 132\,amu$, which becomes more important if one takes the following two facts into account. First, for ^{250}Cf* we have the spectra of postneutron-emission fragment masses. Second, there is a two-units difference in the masses of the fissioning nuclei compared. The difference discussed, is also clearly seen between the mean TKE - FF mass ($< TKE >$-M) distribution (Fig. 5a) and the variance of the TKE distribution for the FF mass given, $\sigma^2(TKE|M)$ (Fig. 5b). The sharp growth of the variance is known to be caused by the multicomponent structure of the distribution. The variance is the higher the larger the distance between the component centers is.

The obtained data on the TKE-M distribution of Cf isotopes permit more definite conclusions compared to [16]. In particular, we can contend, that in the FF TKE-M distribution of ^{250}Cf* at high energies there is a distinct component which is especially pronounced in the vicinity of $A_H \approx 132\,amu$ and suppressed substantially in the analogous FF distribution of ^{252}Cf.

The low statistical uncertainties of the experimental findings for ^{252}Cf and the preneutron emission character of the mass measured allow us to make the following analysis of the proton odd-even effect for different prescission configurations of the fissioning system. At every given TKE value the FF mass-yield spectrum $P(M|TKE)$ is equal to the sum of the Gaussian-like isotope distributions $P(M|Z)$. The approximately five-amu structure observed in the mass yields at low fragment excitation energies, being linked to preference for even charges is known as a proton odd-even effect. To visualize the odd-even

effect in the TKE-M plane we smoothed the original TKE-M distribution and then subtracted this smoothed distribution from the initial one. Fig. 6 displays the plot of the fine-structure obtained in this way for ^{252}Cf FF. The vertical ridges of the plot correspond to the tops of the isotope distributions. The analogous structures are shown in [17] for the ^{235}U(n_{th},f) reaction. In order to relate the ridges to specific FF charges the data of Ref. [10] were used, in which the isotope distributions of ^{252}Cf FF were measured for high TKE values. Two peculiarities of Fig. 6 have to be stressed. The first is that the ridges corresponding to the even-charge splits are vertical over the entire TKE range. It means that the FF neutron-proton ratio N/Z for primary fragments is not influenced by deformation at the scission point. Second, a sharp change in the proton odd-even effect is observed at FF excitation energy $E^* > 40\,MeV$. Below this borderline there appear odd-charge ridges concurrent with those produced by even charges (the most pronounced ones are marked by arrows in Fig. 6).

In order to make the most informative comparison of the experimental findings and theoretical predictions the characteristics of the phenomenon studied should be described in the same or similar coordinates. The choice of such coordinates suitable to both descriptions is a nontrivial task. Usually in calculations dealing with system's evolution from the ground state to scission, an elongation and mass-asymmetry variable are chosen. An excitation energy E^* which is proportional to system elongation and obtained using experimental data seems to be a more appropriate choice than TKE. The TKE - values depend not only on the fragment intercenter distance but on the $Z_L \times Z_H$ charge product as well. An additional advantage of using E^* as a variable consists in natural inclusion of a priori information about energy release $Q(M_L, M_H)$ into consideration. One more aspect should be taken into account. Bearing in mind the present-day progress of theory, the absolute FF yields are less preferable for analysis than the corresponding relative values. The latter fact is due to the complexity of quantitative description of fission modes population and to inadequate definition of the scission criterion.

With the above-said in mind, the experimental TKE-M distribution of ^{252}Cf FF was transformed to the conditional distribution $P(M|E^*)$. It can be done by normalization to unit (100%) area of every cross section at given E^* of the $P(M, E^*)$ distribution.

According to the probability theory [18], by definition,

$$P(M|E^*) = P(M, E^*)/P(E^*),$$

where $P(E^*) = \sum_M P(M, E^*)$. The contour map of the $P(M|E^*)$ distribution presented in Fig. 7 gives a vivid presentation of the regression-like links between the M and E^* variables. One can clearly see the two components with a transition region between them at $E^* \approx 40\,MeV$. The components are labeled by letters A and B.

4 Results of the potential energy surface calculations

To analyze the mass-energy distribution of FF for ^{252}Cf and ^{250}Cf* the PES calculations were performed. The deformation energy of the nucleus was obtained using the Strutinsky method [19] with a Woods-Saxon-like potential [20]. The nuclear shape was parameterized in the coordinate system based on Cassini ovals as one of the coordinate line families [21]. The liquid-drop component of the energy was considered in the frame of the conventional liquid drop model with a sharp surface with parameters taken from [22], and the Krappe-Nix model with a diffused surface as well [23].

Minimizing the potential energy for the deformation parameters one obtains PES as a function of elongation and mass-asymmetry. The resultant PES shows some separate valleys.

The potential energy of the fissioning ^{252}Cf nucleus as a function of its quadrupole moment, $Q = R_0^{-5} \int_{z_L}^{z_R} r^2(4z^2 - r^2)\,dz$ [21], is presented in Fig. 8 for the points along every valley bottom.

As the analysis of the valleys marked by 1 and 4 in Fig. 8 is in progress now [24], so these valleys will not be discussed in this paper.

At the initial stages of quadrupole deformation the nuclear shape can be presented as two partly overlapping spherical nuclei (Fig. 8a) with masses $\approx 132\,amu$. With a further system elongation a jump to the mass-asymmetric configuration takes place (Fig. 8b). This configuration looks like the spherical ^{134}Te nucleus smoothly connected with the deformed $^{80-82}$Ge by a thick neck. The quadrupole deformation of the latter, $\beta \approx 0.1$, lies in the region of the maximum shell correction values (see Fig. 1 in [25]).

For the reasons explained below, we shall call as clusters the two constituents coincide with magic nuclei by the shape and composition and separated geometrically in the fissioning system. Their nucleon compositions are the same as those of Te and Ge nuclei in this case. A spherical cluster with the mass of $\approx 60\,amu$ (it is supposed to be $^{60}_{28}$Ni) fits well into the shape of the Ge nucleus.

At large elongations (Fig. 8c) the fissioning system looks as the $^{128-132}$Sn nuclei linked to the light nascent fragment having a rather peculiar shape. This nascent fragment can be described by means of the following nuclear shape hierarchy: ^{60}Ni$\rightarrow^{80}$Ge$\rightarrow^{96}$Sr$\rightarrow^{106}$Mo. The shapes of ^{80}Ge and ^{96}Sr nuclei are close to their ground state shapes [26]. For ^{96}Sr the equilibrium deformation is similar to the one characterizing the BB' shell-loci in [25]. and deformation of the ^{106}Mo nuclei corresponds to the centers of CC'-shell-loci. In forthcoming discussion we shall call the states of the fissioning system close by shape to those presented in panels in Fig. 8 as modes. This modes will be labeled below by letters (a)-(d) respectively.

With the elongation of the fissioning system the shape of the light cluster follows at first the shape of ^{60}Ni (sphere), then ^{80}Ge ($\beta \approx 0.1$) , then ^{96}Sr ($\beta \approx 0.35$) and that of ^{106}Mo ($\beta \approx 0.55$). The last phase shown in Fig. 8c corresponds to the light fragment elongation which is equal to the main axis of the deformed magic nucleus of Cd ($\beta_2 \approx 0.85$, KK'-shell [25]).

Thus a light cluster changes its nucleon composition and its shape according to the shell channels $A\,B\,C$ and $B'\,C'\,K'$ of the shell correction maps (Figs. 1 and 2 in [25]).

In the system configuration shown in Fig. 8c the rupture of the neck in its minimum radius region provides a fragment pair with a mass ratio of 134/118. The nucleon composition of the heavy spherical cluster is the same as that of the ^{128}Sn nucleus. In this case, the system shape can be treated as two touching nuclei, Sn and Cd, with their contact area being covered by the neutron "coat" or as two partly overlapping nuclei, Cd and slightly deformed ^{134}Te. For a further consideration it is important for the light fragment to be a magic or even double magic nucleus [27].

There is another mode (marked by 3 in Fig. 8) with an energy and shape close to the previous one. It originates in the vicinity of the state, shown in Fig. 8b. As it can be seen this nuclear shape is also dumb-bell-like, but the squeeze point in the neck is formed on

the side of the light cluster (^{106}Mo) rather than of the heavy one (^{134}Te) (Fig. 8d).

The characteristic hierarchy of magic nuclei shapes observed as the light cluster shape in the 2nd and 3rd modes manifests itself also in the fissioning nucleus shape in the 4th valley. Similar results have been obtained for ^{250}Cf as well.

The results at hand are in conceptually agreement and substantially improve the understanding of the nature of multymodelity in comparison with the results [28] for the cluster correlations in the fission of actinide nuclei.

5 Discussion

The first peculiarity of FF mass-energy spectra mentioned above is associated with cold fragmentation (CF), i.e. fission events occurring at TKE values close to Q. CF products are expected to be produced in slightly deformed states close to the ground state. Up to now the problem of correlation between the characteristics of CF products and the shape of the fissioning system where CF starts remains poorly investigated. Just this problem should be analyzed at least qualitatively, in order to interpret the data being discussed.

Bearing in mind that light fragments complementary to heavy ones around $M_H \approx 132\,amu$ (the region of the "bump" - see Figs. 3. 4, 5) are almost spherical in the ground state, the most "cold" fission involving such FF pairs can be expected to occur in the states shown in Fig. 8a. However in spontaneous fission these states are skipped over, in other words, the exit point for subbarrier tunneling corresponds to the system elongation at which mode (a) has already disappeared (Fig. 8). It should be noted that the latter statement is principally important. There is a sharp boundary for fissioning nucleus elongation within this mode. In fact, if the system consists of two independent $^{132}_{50}$Sn nuclei being in contact, it should be $^{264}_{100}Fm$ in composition. If the Sn nuclei begin to overlap in the sense that nucleons become "common" in the region of overlapping, the ^{252}Cf nucleus can be formed at some stage of system elongation (overlapping). Similar situations have been formerly analyzed in the framework of the two-center potential model [29].

Nevertheless another opportunity of the manifestation of this mode cannot be rejected a priori. The tunneling from the ground state of ^{252}Cf directly to the valley of separated fragments can occur. This is just the valley where ^{250}Cf* CF products are formed from the

states called as the mode (a). An increase of the variance of the $P(TKE|M)$ distribution around $M_H \approx 132\,amu$ can be due to cold fission through the states of mode (a) for both ^{250}Cf* and ^{252}Cf. The results of Ref. [1], where the true cold fission has been observed for FF the pair ^{132}Sn/^{120}Cd seem to confirm this assumption. Thus, the "bump" observed in the TKE-M distribution of ^{250}Cf* FF emerges presumably as a result of the difference in the probabilities of tunneling into the valley of separated fragments from the ground state of ^{252}Cf and from the states of ^{250}Cf* belonging to the mode (a). In the latter case the probability of tunneling is determined not only by barrier penetrability but also by the time of passing through the states of the mode (a). As the mode (b) shapes are more prolate (Fig. 8b), at the initial stage of the descent fission will be more "deformed" in this mode, i.e. the TKE of the fragments formed will be far apart from the limiting values, determined by Q, as compared to the mode (a).

Another consequence is that the group of ^{252}Cf FF formed around $M_H \approx 140\,amu$ prevail in the yields at low E^*. The light fragments of this group have significant ground state deformations [26].

An interpretation of the other results mentioned in section 3 will be more illustrative. We emphasize a very good agreement between the ^{252}Cf fission scenarios obtained from calculated results (Fig. 8) and the experimental $P(M|E^*)$ distribution contour map (Fig. 7). As noted above, in the CF region pairs prevail around the mass split 110/140 (Fig. 7). In this figure the point where bifurcation of ridges is seen corresponds to that phase of the system evolution where the ^{106}Mo cluster is just formed, and a flat neck connects it with the heavy fragment. At the following stage the neck will be fastened near the light Mo cluster (component A) or near the heavy Te cluster (component B) (Fig. 7), corresponding to modes (d) and (c) in Fig. 8. On the basis of the contour map one can conclude that ruptures occur in component A near the Mo cluster, and the system becomes more prolate at expense of the neck. If, in accordance with theoretical prediction for mode (c), the heavy fragment is really a spherical cluster, it has to stay unexcited in spite of a very high total excitation of the fissioning system. This is confirmed by Fig. 9 where the contour map of the $P(M|E^*)$ distribution for ^{250}Cf* FF is presented. Thus the heavy fragment does not really emit neutrons, as the masses are measured for ^{250}Cf* after neutron emission. Unfortunately, the coordinates used in Figs. 7 and 9 can not be used in

the case of neutron emission. Therefore the light peak observed in FF mass distribution for $^{250}Cf^*$ cannot be analyzed in the same way.

The data presented in Fig. 6 can be treated as those directly related to clustering. As was mentioned in section 4, the light cluster follows the shell channel A, BB', CC' of the shell correction map [25] as the system elongates. At $E^* > 40\,MeV$, where mode (c) (Fig. 8) prevails, the fissioning system is likely to undergo complete clustering. As noted in section 4, the system is composed of two touching magic nuclei, deformed Cd and spherical Sn (Te). No correlations of superconducting type are known to exist in cold magic nuclei [30]. Just this fact can lead to the sharp decrease of the proton odd-even effect, being detected by fine-structure in the TKE-M distribution shown in Fig. 6.

6 Summary

The present study has given reliable evidence for the dicluster mechanism of fission mode formation, first proposed in Ref. [31, 32].

The results of the PES calculations for $^{250}Cf^*$ and ^{252}Cf nuclei demonstrate the presence of several potential energy valleys. Two geometrically invariable constituents, which are close to magic spherical and deformed nuclei in composition and shape, are responsible for the shape of the fissioning system in each fission valley. The observed peculiarities of the shape of the fissioning system allow us to assume that they are due to clustering.

As a result of the PES calculations, it has established that there exist two distinct fission modes produced by the Sn and Mo clusters. At great elongations the two modes differ in the location of the area where rupture takes place with the highest probability: near the heavy or light cluster. In the experimental data obtained the modes manifest themselves as two well separated components in the $P(M|E^*)$ distribution. The slight excitation of the heavy cluster, expected at the limiting elongation of the fissioning system, is confirmed by the structure of the $P(M|E^*)$ distribution of the heavy fragments produced in $^{250}Cf^*$ fission.

Crucial evidence for the clustering of the fissioning system is provided by the complete clusterization of the system volume, which is observed in the form of an abrupt drop (or possible disappearance) of the proton odd-even staggering in the corresponding fission mode.

a)

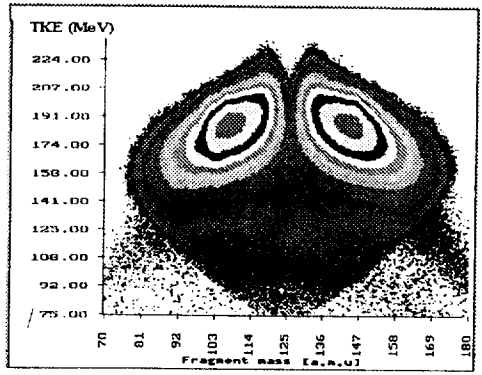

b)

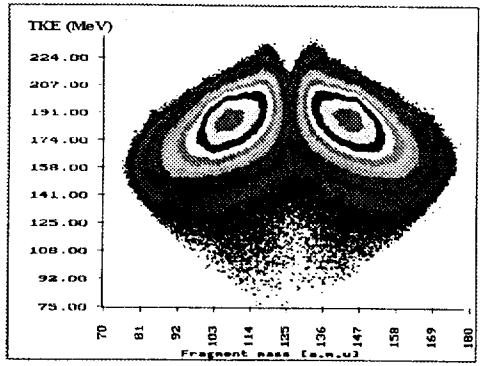

Fig. 1 The total kinetic energy-mass (TKE-M) distribution of fission fragments obtained by TOF-TOF analysis. The upper part (a) contains all events and in the lower part (b) only such events are included which give consistent results in TOF-TOF and TOF-E analysis.

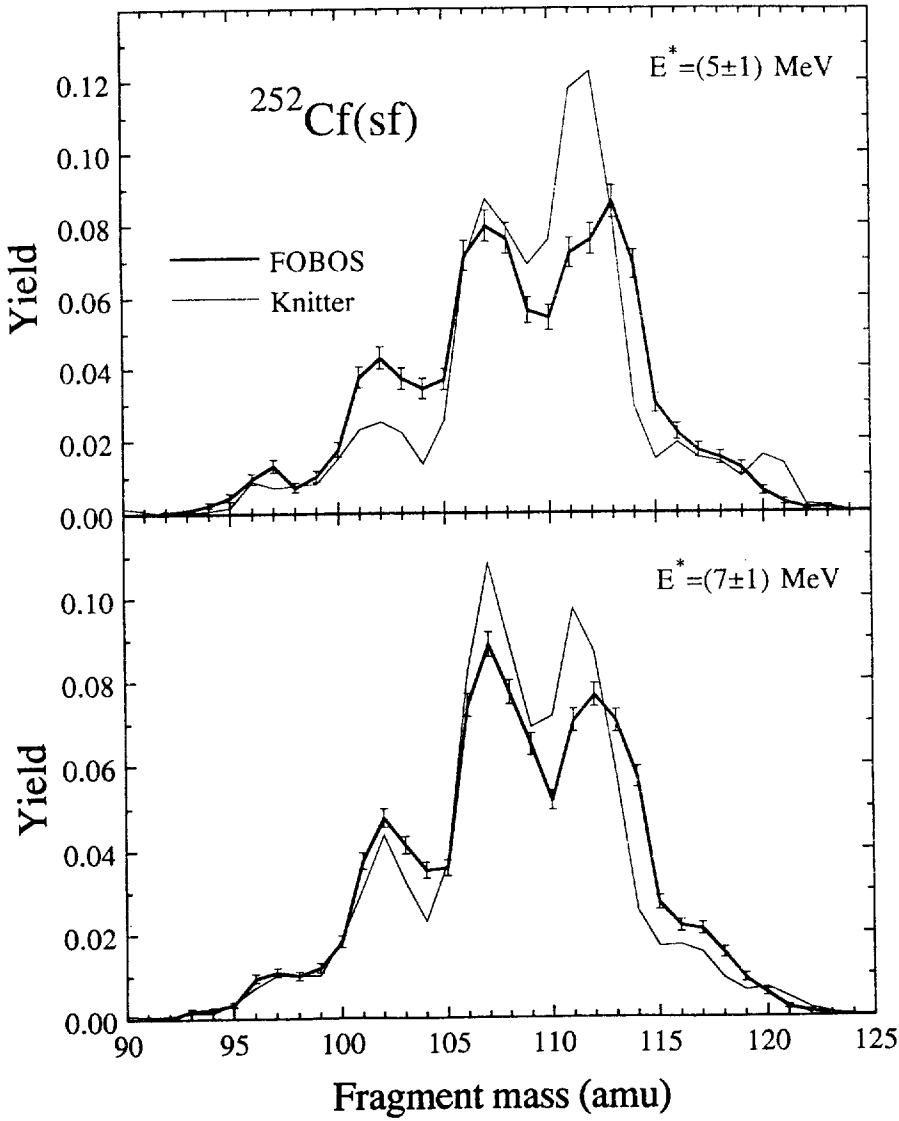

Fig. 2 ^{252}Cf FF mass spectra obtained in Ref. [10] and in this work for two selected excitation energy corridors. The yield sums are normalized to unity.

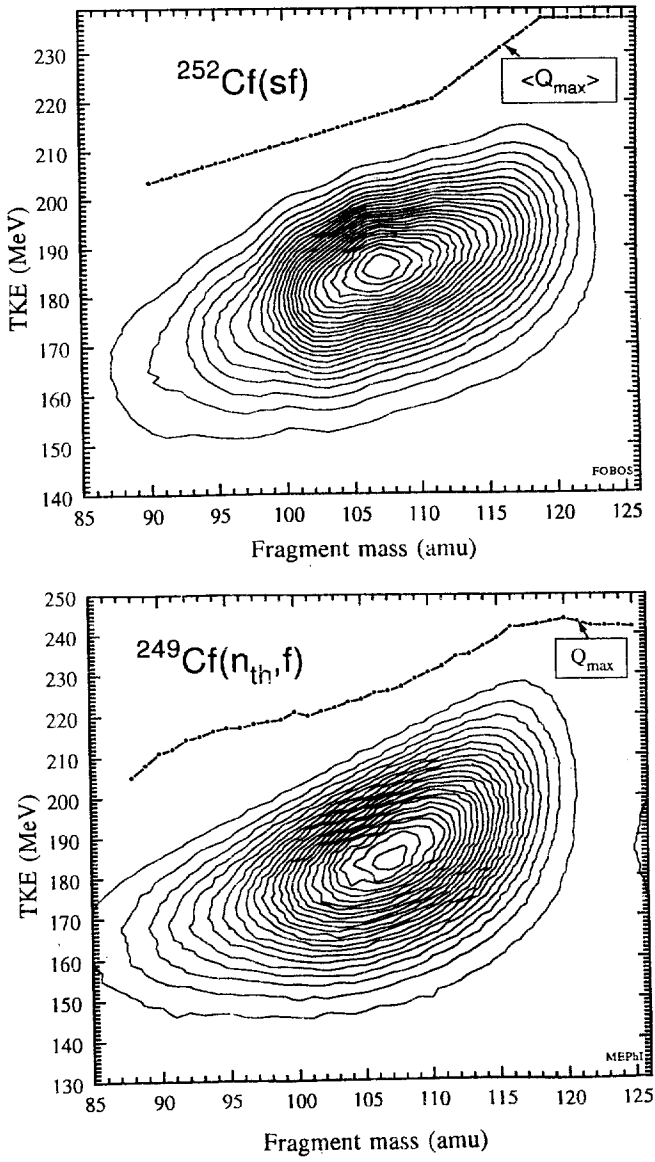

Fig. 3 The contour map of TKE-M distribution for light ^{252}Cf FF. The distance between subsequent contour lines corresponds to 4% of maximum yield.

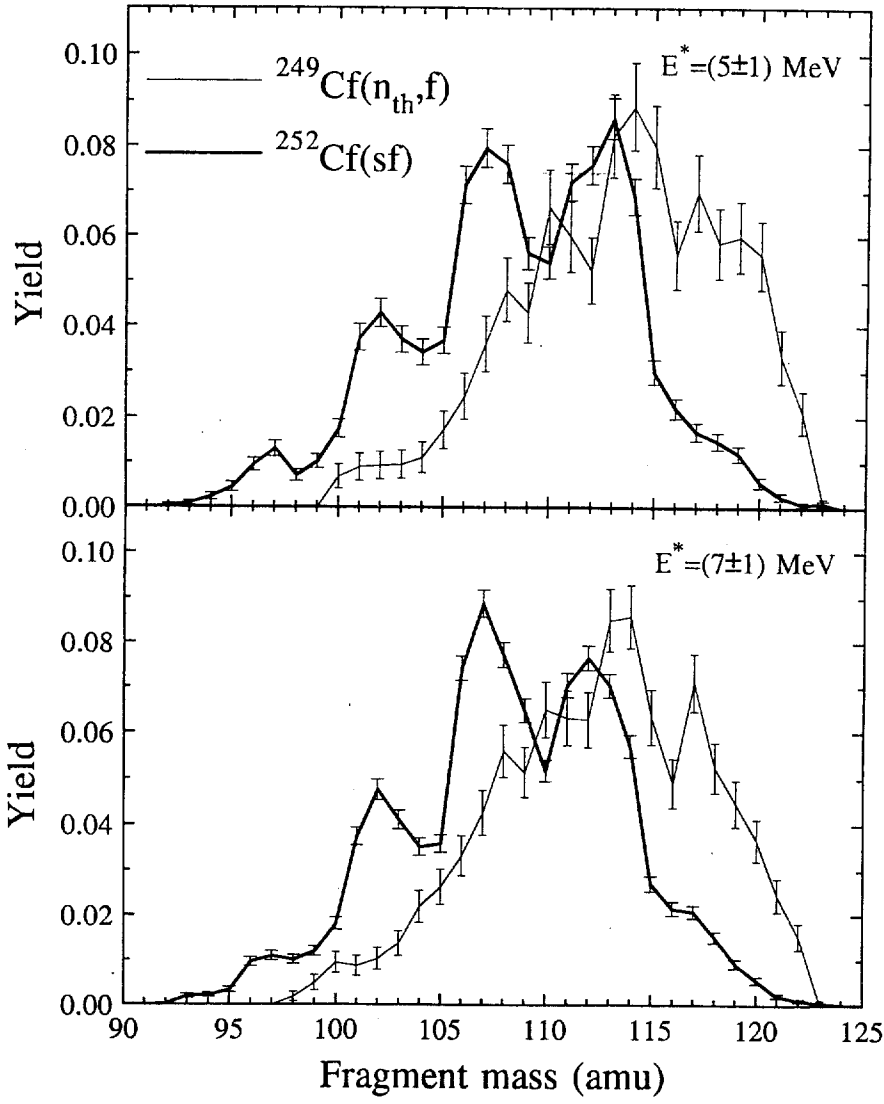

Fig. 4 Comparison of FF mass spectra from ^{252}Cf(sf) and ^{249}Cf(n_{th},f) reactions for two distinct excitation energy corridors.

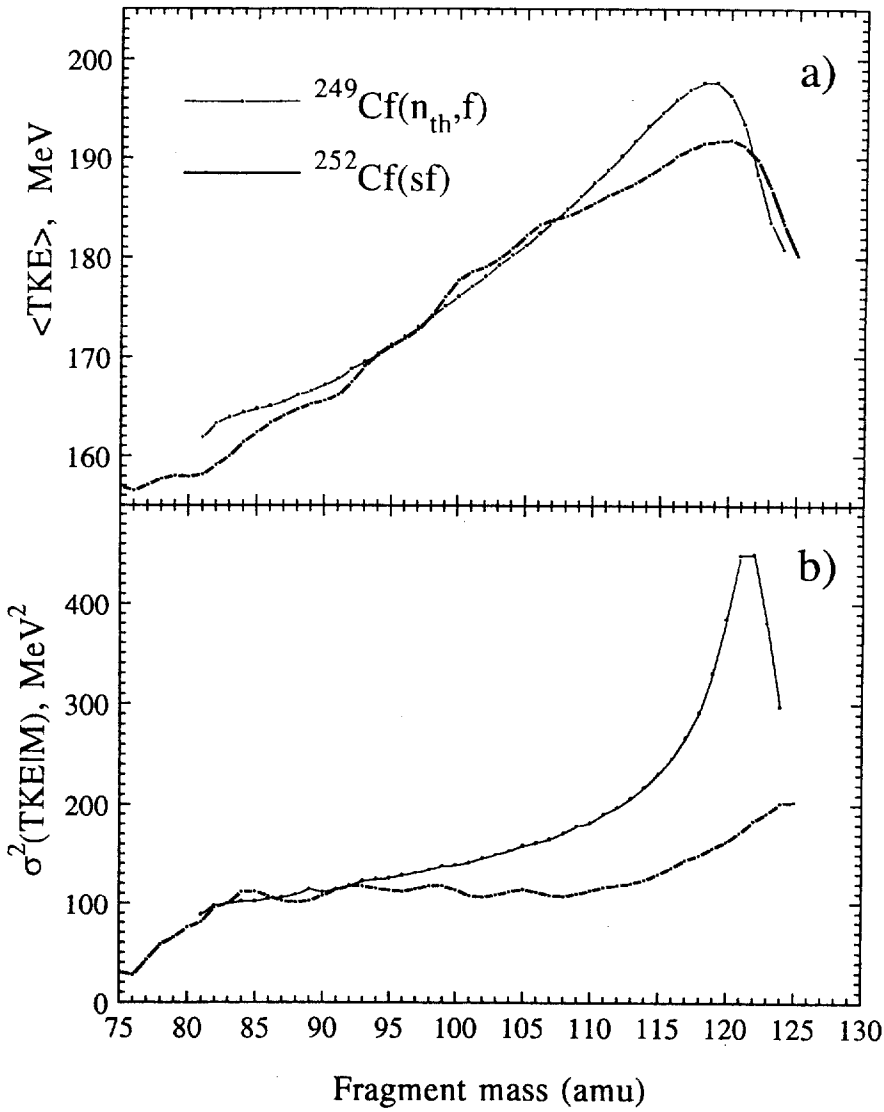

Fig. 5 Mean TKE (a) and TKE variance (b) as a function of the selected mass splits.

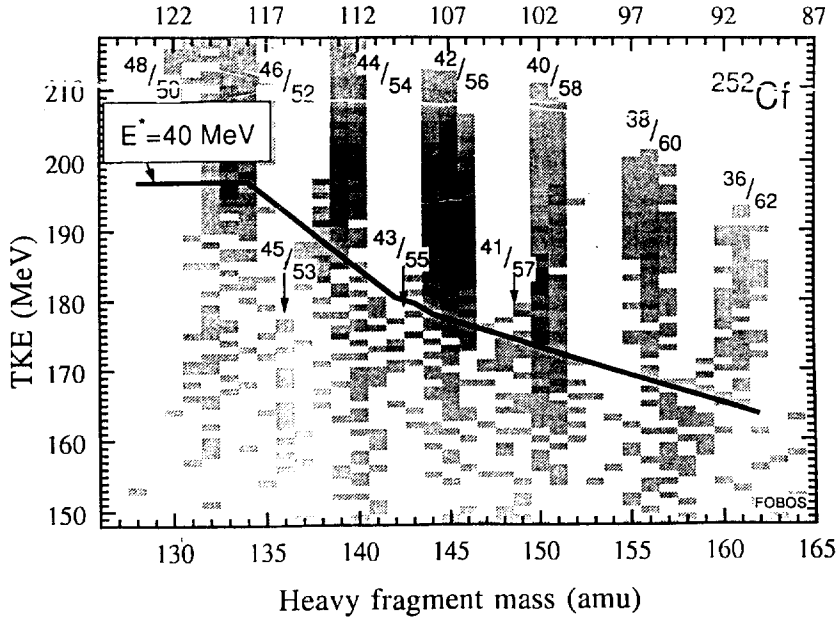

Fig. 6 The fine structure of the TKE-M distribution of ^{252}Cf FF demonstrating the proton odd-even staggering. For details, see the text.

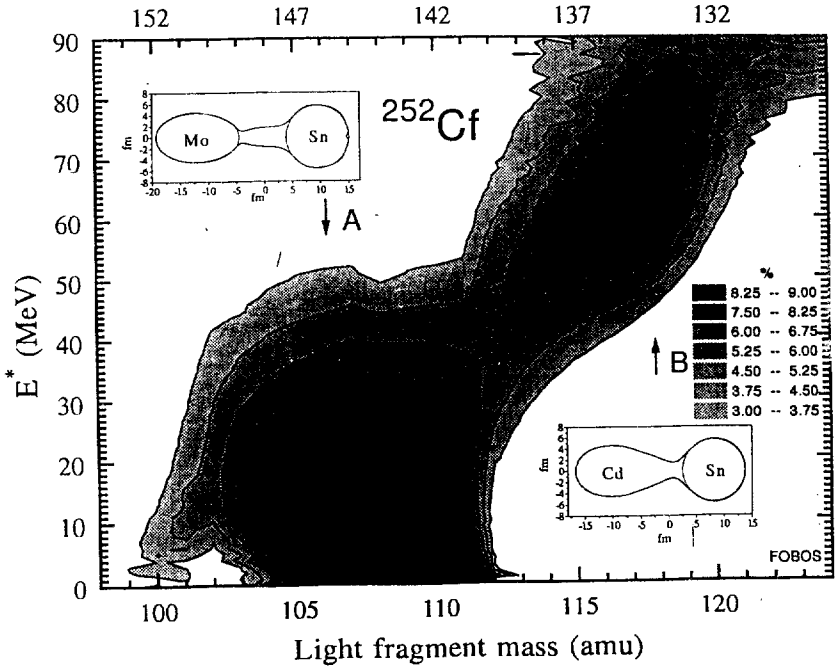

Fig. 7 The contour map of the conditional distribution $P(M|E^*)$. The panels depict the shapes of the fissioning system following from the PES calculations ascribed to the two dominant structures.

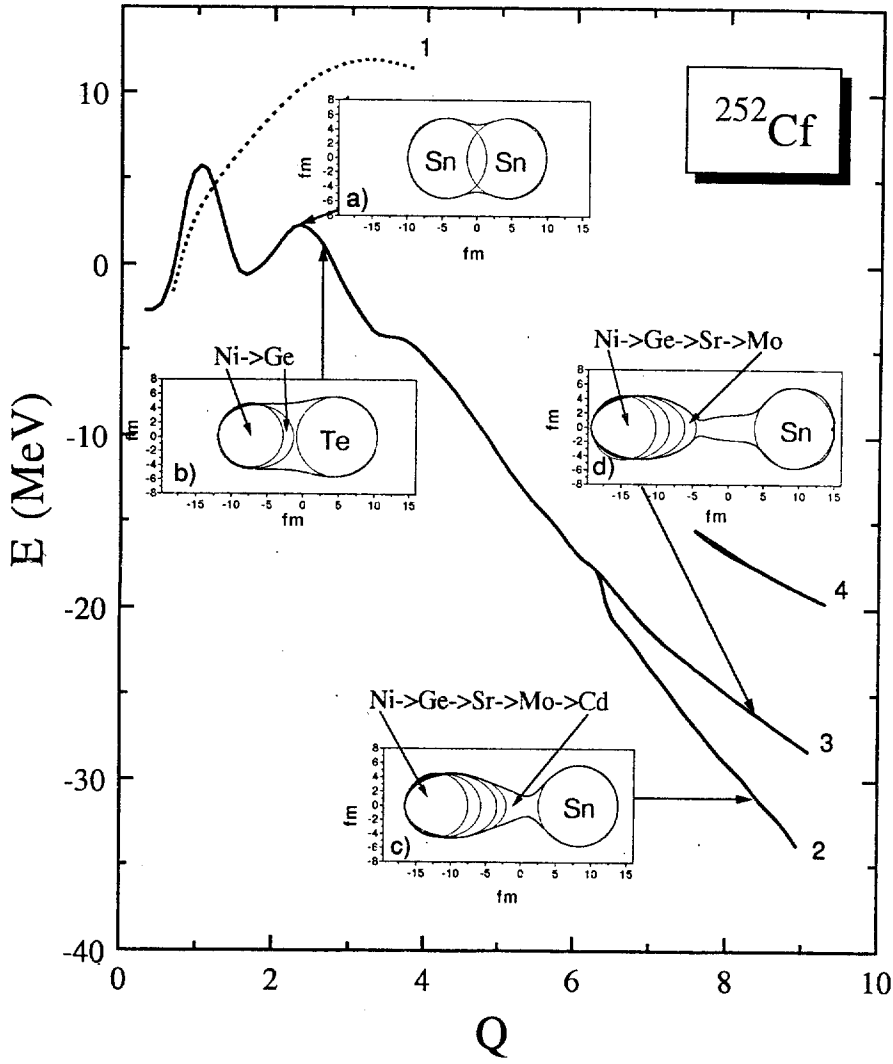

Fig. 8 Potential energy of the fissioning nucleus ^{252}Cf corresponding to the bottoms of the potential valleys, as a function of its quadrupole moment Q. The valleys found in the PES calculations are marked by numbers 1 to 4. The panels depict the shapes of the fissioning system at the points marked by the arrows.

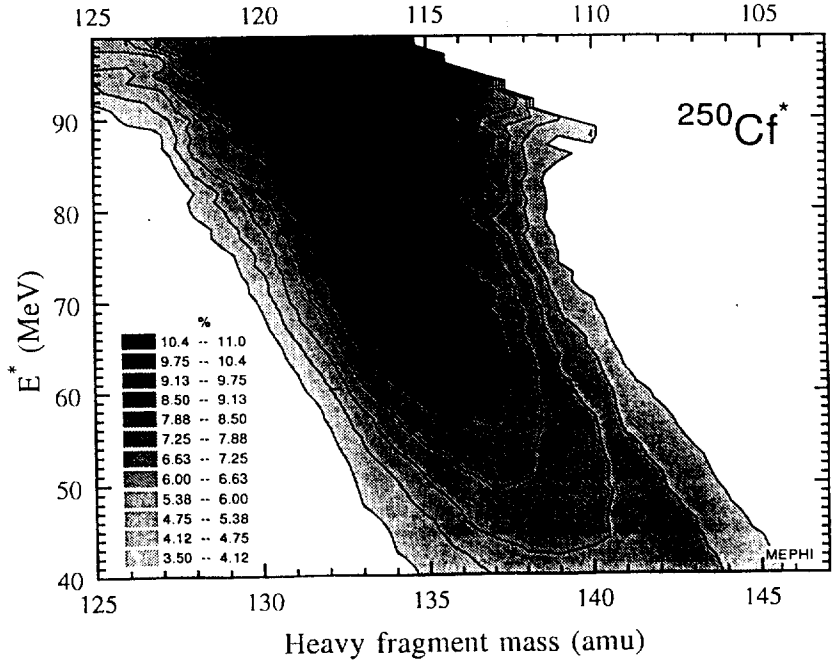

Fig. 9 The contour map of the conditional distribution $P(M|E^*)$ for the heavy fragments produced in $^{250}Cf^*$ fission.

This work is supported in part by Russian Foundation for Basic Research, grant 96-02-17674.

References

[1] F. Gönnenwein *et al*, Proc. XIII Meeting on Physics of Nuclear Fission in memory of prof. G.N. Smirenkin, Obninsk, 1995, ed. A.V. Ignatyuk (in press).

[2] G.M. Ter-Akopian, J.H. Hamilton, Yu.Ts. Oganesian, A.V. Daniel, J. Kormicki, A.V. Ramayya, G.S. Popeko, B.R.S. Babu, Q. Lu, K. Butler-Moore, W.-C. Ma, S. Cwiok, W. Nazarewicz, J.K. Deng, D. Shi, J. Kliman, M. Morhac, J.D. Cole, R. Aryaeinejad, N.R. Johnson, I.Y. Lee, F.K. McGowan and J.X. Saladin, Phys. Rev. Lett. 77 (1996) 32.

[3] H. Märten, Proc. of the Int. Workshop "Dynamical Aspectes of Nuclear Fission", Smolenice, Czechoslovakia, 1991, ed. B.I. Pustylnik (Dubna, E7-92-95, 1992) p. 32.

[4] U. Brosa, S. Grossman and A. Müller, Phys. Reports, vol. 197 (1990) 167.

[5] F. Gönnenwein and Börsig, Nucl. Phys. A 530 (1991) 27.

[6] A. Florescu, A. Sandulescu, C. Cioca and W. Greiner, J. Phys. G: Nucl. Phys. 19 (1993) 669.

[7] J.F. Berger, M. Girod and D. Gogny, Nucl. Phys. A 428 (1984) 230.

[8] M. Andrassy *et. al.* (FOBOS collaboration) Communication of JINR, Dubna, Russia E7-95-148, 1995.

[9] S.L. Podshibyakin, Yu.V. Pyatkov, A.I. Slyusarenko and A.N. Shemetov, Pribory i Technika Eksperimenta 6 (1988) 78 [in Russian].

[10] M.H. Knitter, F.-J. Hambsch and C. Budtz-Jørgensen, Nucl. Phys. A 536 (1992) 221.

[11] Yu.V. Pyatkov, R.A. Shekhmametiev and A.I. Slyusarenko, JINR Rapid Communications 2 (1993) 98.

[12] A.A. Alexandrov, I.A. Alexandrova, A.V. Ermolenko, Yu.K. Korjuk, D.S. Nikulin, Yu.F. Pevchev, S.L. Podshibyakin, Yu.V. Pyatkov, S.I. Sitnikov, A.I. Slyusarenko, A.N. Shemetov and R.A. Shekhmametiev, NIM A 303 (1991) 323.

[13] S.L. Podshibyakin, Yu.V. Pyatkov and A.N. Slyusarenko, Experimental Methods in Applied and Fundamental Nuclear Physics, ed. Yu.V. Pyatkov (Atomizdat, Moscow, Russia, 1991) p. 19.

[14] A.A. Alexandrov, I.A. Alexandrova, S.L. Podshibyakin et al., NIM A 302 (1991) 178.

[15] M. Djebara, M. Asghar, J.P. Bocquet, R. Brissot, J. Crancon, Ch. Ristori, E. Aker, D. Engelhardt, J. Gindler, B.D. Wilkins, W. Quade and K. Rudolph, Nucl. Phys. A 496 (1988) 346.

[16] Yu.V. Pyatkov and R.A. Shekhmametiev, Second Int. Conf. on Dynamical Aspects of Nuclear Fission Smolenice, Slovakia, 1993, ed. B.I. Pustylnik (Dubna, 1994) p. 236.

[17] A.A. Alexandrov, I.A. Alexandrova, S.L. Podshibyakin, Yu.V. Pyatkov, A.I. Slyusarenko, A.N. Shemetov and R.A. Shekhmametiev, Proc. Int. Conf. "50-anniversary of Nuclear fission", Leningrad, 1988, ed. G. Petrov p. 388.

[18] G.A. Korn and T.M. Korn, Mathematical Handbook for Scientists and Engineers (New York, Toronto, London, 1961).

[19] V.M. Strutinsky, Nucl. Phys. A 95 (1967) 420.

[20] V.M. Strutinsky, Nucl. Phys. A 122 (1968) 1.

[21] V.V. Pashkevich, Nucl. Phys. A 477 (1988) 1.

[22] W.D. Myers and W.J. Swiatecki, Ark. Fys 36 (1967) 343.

[23] H.J. Krappe, N.R. Nix and A.J. Sierk, Phys. Rev. Lett. 42 (1979) 215.

[24] Yu.V. Pyatkov, A.V. Unzhakova, V.V. Pashkevich and V.G. Tishchenko, Izv. RAN, ser. fiz., 1996, [in Russian] (in press).

[25] B.D. Wilkins, E.P. Steinberg and R.R. Chasman, Phys. Rev. 14 (1976) 1832.

[26] P. Möller and R.J. Nix, Atomic Data and Nuclear Data Tables 26 (1981) 165.

[27] H. Märten (private communication).

[28] S. Cwiok, W. Nazarewicz, J.X. Saladin, W. Plociennik and A. Johnson, Phys. Letters B 22 (1994) 304.

[29] J. Maruhn, W. Scheid and W. Greiner, in "Heavy Ion Collisions", ed. R. Bock, vol. II (North Holland, Amsterdam, 1980).

[30] V.G. Soloviev, Theory of Atomic Nucleus (Moscow, Energoatomizdat, 1981).

[31] Yu.V. Pyatkov, R.A. Shekhmametiev, A.I. Slyusarenko and A.V. Taranenko. Proc. of the Int. Conf. on Nuclear Structure and Nuclear Reactions at Low and Intermediate Energies, Dubna, 1992, ed. R.V. Jolos (Russia, Dubna, 1993) p. 347.

[32] Yu.V. Pyatkov and R.A. Shekhmametiev, Phys. of Atomic Nuclei 57 (1994) 1182.

Received by Publishing Department
on October 7, 1996.

Пятков Ю.В. и др. E15-96-365

Проявления кластеризации в реакциях ^{252}Cf (sf) и ^{249}Cf (n_{th},f)

На базе расчетов поверхностей потенциальной энергии проведен сравнительный анализ массово-энергетических распределений осколков деления в реакциях ^{252}Cf (sf), ^{249}Cf (n_{th},f). Полученные экспериментальные и теоретические результаты указывают на существование делительных мод, обусловленных кластеризацией делящихся ядер. Обнаружено резкое уменьшение величины протонного четно-нечетного эффекта для возбуждения в точке разрыва $E^* > 40$ МэВ, что предположительно связано с полной кластеризацией делящегося ядра в одной из мод.

Работа выполнена в Лаборатории ядерных реакций им.Г.Н.Флерова и Лаборатории теоретической физики им.Н.Н.Боголюбова ОИЯИ.

Препринт Объединенного института ядерных исследований. Дубна, 1996

Pyatkov Yu.V. et al. E15-96-365

Manifestation of Clustering in the ^{252}Cf (sf) and ^{249}Cf (n_{th},f) Reactions

A comparative analysis of the mass-energy distribution of the fission fragments formed in ^{252}Cf (sf) and ^{249}Cf (n_{th},f) reactions is performed on the basis of the potential energy surface calculations. The available experimental and theoretical results give evidence for the existence of fission modes caused by clustering of the fissioning nuclei. A sharp drop of the proton odd-even effect is discovered at excitation energy in the scission point $E^* > 40$ MeV, which is presumably associated with the complete clusterization of the fissioning nucleus.

The investigation has been performed at the Flerov Laboratory of Nuclear Reactions and Bogoliubov Laboratory of Theoretical Physics, JINR.

Preprint of the Joint Institute for Nuclear Research. Dubna, 1996

Макет Т.Е.Попеко

Подписано в печать 02.12.96
Формат 60 × 90/16. Офсетная печать. Уч.-изд.листов 2,28
Тираж 290. Заказ 49541. Цена 2736 р.

Издательский отдел Объединенного института ядерных исследований
Дубна Московской области